# Geometric effects on competing failure modes in lap shear testing of spot joints

Tushar Telmasre<sup>1</sup>, Abdelrahman Abdelmotagaly<sup>1</sup>, Gao Yanfei<sup>2</sup>, Yu Zhenzhen<sup>1</sup>
Tushar Telmasre, Abdelrahman Abdelmotagaly, 高雁飞, 于真真

- 1. Department of Metallurgical and Materials Engineering, Colorado School of Mines, Golden, CO 80401, USA;
  - 2. Department of Materials Science and Engineering, University of Tennessee, Knoxville, TN 37996, USA

Received 16 June 2022; accepted 23 July 2022

Abstract When subjected to the lap shear testing, spot welds created by brazing, resistance welding, or other techniques may fail either by a plug failure mode (also called pull-out mode) or an interfacial shear failure mode. In the past, plug failure mode was thought to be dependent on base metal ultimate tensile strength, spot diameter and plate thickness, while interfacial failure can be determined by interface shear strength and spot area. No fracture mechanics model or failure process is invoked in such an approach, and its predictive capability is often doubted compared to realistic experiments. This work conducts a parametric study to assess the failure behavior as a function of dominant three-dimensional geometric parameters based on the Gurson-Tvergaard-Needleman (GTN) damage mechanics model and no-damage model respectively. Different necking conditions are considered as precursors to the two failure modes in the no-damage model. It is found out that a small ratio of spot diameter to plate thickness promotes interfacial shear failure while a large ratio favors plug failure. Other geometric parameters such as the filler interlayer thickness, if used, play a secondary role. The calculated peak force  $F_{wt}$  is not much different between the GTN and no-damage analyses, and better agreement is shown in the small nugget region. Normalized peak force calculated from the GTN model with the porosity  $f_0$  set to 0.01 showed the best agreement with pervious tensile shear tests on spot-welded DP980 lap joints in comparison to that calculated from the GTN model with  $f_0$  at 0.02 and the no-damage model. Note that heterogeneous distribution of material strength across the joint region was considered in the GTN model, which was estimated based on the hardness map measured across the joint cross section.

Key words spot welding, failure modes, damage mechanics

## 0 Introduction

For lap joints and spot welds, a sound metallurgical bond with good strength can be generated by selecting appropriate fillers and joint designs<sup>[1-3]</sup>. Since the base metals, filler materials and weld quality all contribute to the overall failure strength of the joints, the deformation behavior could be complex to understand, leading to challenges in optimization of failure strength and toughness. Lap shear test is the most commonly used technique for such a purpose. The

boundary value problem results in the development of a nonuniform stress field in the joint region, which makes it difficult to attribute failure strength to either the interlayer strength or the base metal strength alone [4-6].

It was suggested by multiple researchers that in lap joints an approximately uniform stress can be developed in the interlayer for small overlaps. Besides, for larger overlaps, a high stress concentration is developed near the two lap ends<sup>[6–8]</sup>. In other words, the interlayer is constrained by the two base metal plates, and thus develops a complex triaxial stress state<sup>[9–10]</sup>. Such behaviors correspond to the two

**Foundation item:** This research was supported by National Science Foundation (NSF) with Award No. 1847630 and used experimental data generated from a project supported by Honda R&D Americas, Inc. (Raymond, OH) to the team at Colorado School of Mines, and by NSF Grant 1822186 to the University of Tennessee.

Corresponding author: Yu Zhenzhen, Ph.D., Associate Professor. Mainly engage in weld metallurgy and weld consumales design. E-mail: zyu@mines.edu

doi: 10.12073/j.cw.20220616001

distinct types of failure modes, including the interfacial shear failure (i.e., shearing of the interlayer like a sliding process) and the pull-out failure (i.e., fracture in base metal plates near the joint region, also known as plug failure). The dominating factor for the transition of these two modes from one to the other has been identified as the overlap in two-dimensional or the nugget size in three-dimensional setups [11-12]. Pouranvari et al. [13] reported a threshold value of r=2t for resistance spot welds of steels, where r is the radius of nugget and t is the thickness of the plate. As t 2t, the shear stress was nearly uniformly distributed in the interlayer, and interfacial failure was observed, while as t 2t, high stress concentration developed in the base metal region on the periphery of the joint associated with rotation of the joint.

The fracture strength of a pull-out or plug failure mode was believed to be usually higher than that of interfacial mode. Experiments on Al-Si coated press hardened steel<sup>[14 - 15]</sup>, low carbon steels<sup>[16]</sup>, advanced high-strength steels<sup>[17]</sup>, and many others have corroborated that with increasing nugget size, the failure mode switches from interfacial to pull-out, and results in an overall increase in fracture strength. Furthermore, in our previous tensile shear experiments on spot-welded lap joints of galvannealed DP980 steel using a high-entropy-alloy (HEA) filler [18], the thickness of interlayer filler was varied from 220 to 370 µm to investigate the effect of interlayer thickness on the failure mode as well as the peak force of tensile shear tests. When the experiments were conducted without an interlayer, the failure mode was predominantly interfacial. With the increase in the interlayer thickness, the failure transitioned to a mixed mode where the fracture surface exhibited characteristics associated with both interfacial and pull-out modes. However, the peak force showed a downward trend with the increase in the interlayer thickness. Therefore, more indepth theoretical analysis is needed to fundamentally understand the impact of joint geometry on the synergistic changes of failure modes, peak force, and other experimental findings.

The welding community generally predicts lap-shear strength using two methodologies: simple strength models versus fracture-mechanics based models. The former ones have been widely recommended in welding and joining handbooks due to their easy application and some empirical successes<sup>[19]</sup>. According to the suggestions from American Welding Society (AWS), the critical force corresponding to interfacial shear failure is taken to be proportional to  $\sigma_s D^2$ , where D = 2r is the nugget diameter and  $\sigma_s$  is the interface shear strength. Similarly, the critical force for plug failure is  $\sigma_{UTS} Dt$ , where  $\sigma_{UTS}$  is the ultimate tensile strength of the base metal. These simplified equations can be justified by

the nearly uniform shear stress field at small nugget sizes and the development of nearly full plastic fields. Even without the knowledge of  $\sigma_s$ , comparison of these two equations shows that, provided with a large ratio of D/t, the interfacial shear failure force will be much larger than the plug failure force, so that the plug failure will take place first. This is clearly in line with almost all experimental findings, but further successes have not been achieved, especially for quantitative comparison to experiments. This is because small nugget sizes will lead to plate rotation and thus a combined tensile-shear stress state. To this end, attempts have been made to improve the above equations for combined normal and shear stress components, from which failure mode maps can be developed by comparing these equations<sup>[6]</sup>. There an also more complex models based on the ductility of interlayer, overlap length and thickness, and other parameters<sup>[20-21]</sup> have been proposed.

The other commonly used methodology is fracturemechanics based, such as the linear-elastic-fracture-mechanics (LEFM) approach that compares the stress intensity factor to toughness, and the cohesive zone model that specifies a traction-separation relationship along the weak interface<sup>[19, 22 - 24]</sup>. For example, Zhang et al. <sup>[22, 25]</sup> conducted extensive finite element (FE) simulations and documented the dependence of applied stress intensity factor on various geometric parameters. However, LEFM implicitly assumes that the crack size should be much smaller than the feature sizes in the boundary value problem. This is not the case in welded metal structures, where the plastic zone size is large, and can even extend over the entire lap, which is opposed to the suitable application of the LEFM approach to large structures such as ship decks or composite materials<sup>[26 - 27]</sup>. For cohesive zone approach, although the restriction of failure along certain pre-defined paths can be easily relieved, this method is better suited for modeling adhesive layers and has troubles in modeling the failures in metallic materials<sup>[24, 28]</sup>.

Owing to the limitations of the above two types of models, this work presents failure analyses from a material damage perspective. To be specific, the Gurson-Tvergaard-Needleman (GTN) failure model is adopted here that describes the processes of void nucleation, growth and coalescence [11, 29 - 30]. The voids could be pre-existent, especially within the solidified braze filler region, or nucleated under a high triaxial tension. Using the commercial package, ABAQUS, a detailed FE analysis was performed to understand the effects of geometrical parameters such as radius and thickness of interlayer ( $\geq 0$ ) on the fracture modes of the spot-welded lap joints, as well as their load-bearing capacity. Such a parametric study will allow us to develop a failure-mode map with respect to several dominant dimen-

sionless parameters.

The numerical simulation results will be compared to our lap shear tests on spot welds<sup>[18]</sup> without involvement of brittle phases. Note that some literature experiments on brazed dissimilar metals, such as Ag-CuO<sup>[10]</sup>, Al/Mg<sup>[23]</sup>, Ti6Al4V/Cu/NiTi<sup>[31]</sup> systems, showed a decrease in failure force with an increase in the interlayer thickness. Most of these studies attributed failure to the formation of brittle phases, which act as crack initiation sites. The increase in interlayer thickness led to more volume for detrimental phases to form, and thus adversely affected the fracture strength. In this study, the comparison to experiment without involvement of brittle phases allows for isolation of interlayer thickness effect on stress state change, and therefore will provide validation for the damage-based FE simulations.

#### 1 Problem formulation

For the boundary value problem depicted in Fig. 1, r and d ( $d \ge 0$ ) represent spot weld diameter and filler thickness, respectively. a, t, and w represent overlap distance, plate thickness and width, respectively. F is the force applied during tensile-shear test, we assume power-law hardening for the material, given by

$$\varepsilon = \begin{cases} \frac{\sigma}{E} & \sigma < \sigma_0 \\ \frac{\sigma_0}{E} \left(\frac{\sigma}{\sigma_0}\right)^{\frac{1}{N}} & \sigma \geqslant \sigma_0 \end{cases}$$
 (1)

where E is the Young's modulus,  $\sigma_0$  is yield stress, and N is the strain hardening exponent. As this work aims to compare to experiments by Abdelmotagaly<sup>[18]</sup> where DP-980 steel was the base metal, input database for mechanical properties of DP980 was obtained from literature [18] and tabulated in Table 1. It should be noted that the ultimate tensile strength (UTS) should depend on  $\sigma_0$  and N, since it corresponds to the necking condition under uniaxial tension.

As aforementioned, the GTN damage model is employed for the failure analysis, in which the yield potential is given by

$$\phi = \left(\frac{\sigma_e}{\overline{\sigma}}\right)^2 + 2q_1 f^* \cosh\left(\frac{3q_2\sigma_m}{2\overline{\sigma}}\right) - (1 + (q_1 f^*)^2) = 0 \quad (2)$$

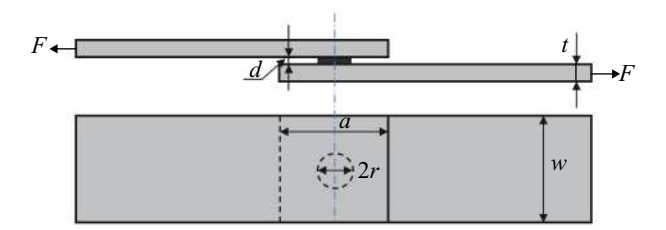


Fig. 1 Schematic illustration of the tensile shear test and the labeling of various parameters involved in the mechanics analysis

where  $\sigma_e$  denotes the effective stress,  $\sigma_m$ the mean stress,  $\overline{\sigma}$  the tensile flow stress representing the actual microscopic stress state in the matrix,  $q_1$  and  $q_2$  are dimensionless parameters to improve agreement between this homogenized model and actual explicit simulations of individual voids. The modified void volume fraction,  $f^*$ , relates to the void volume fraction, f, by

$$f^* = \begin{cases} f & f < f_c \\ f_c + \frac{1}{q_1} - f_c (f - f_c) & f \ge f_c \end{cases}$$
 (3)

where  $f_c$  is the critical value for void coalescence and  $f_f$  is for the final failure. The evolution of void volume fraction are as follows

$$\dot{f} = \dot{f}_{nucl} + (1 - f)D_{kk}^{p} \tag{4}$$

where  $f_{nucl}$  is the nucleation rate and  $D_{kk}^p$  is the sum of principal components of the velocity gradient tensor. The nucleation process is rather complex and oftentimes relies on the knowledge of inclusions and second phase particles. Here for simplicity, we set  $f_{nucl} = 0$  and only consider the initial void volume fraction  $f_0$  as the controlling parameter.

As shown by the FE mesh in Fig. 2, a half model (in y-axis) has been exploited to reduce the computational effort without losing the consistency of the solution for tensile shear tests<sup>[32]</sup>. The variation ranges of parameters defined in Fig. 1 are summarized in Table 2, which are typical sizes for spot joints in automotive applications.

The GTN model has an intrinsic length scale; it is the spacing of voids or void-nucleating inclusions in the material, or the mesh size in FE simulations. According to Tver-

Table 1 Mechanical properties for DP-980 steel, as taken from

Yield strength σ <sub>0</sub> /MPa	Young's modulus E/GPa	Ultimate tensile strength $\sigma_{\rm UTS}/{\rm MPa}$	Strain hardening exponent N
610	190	970	0.37

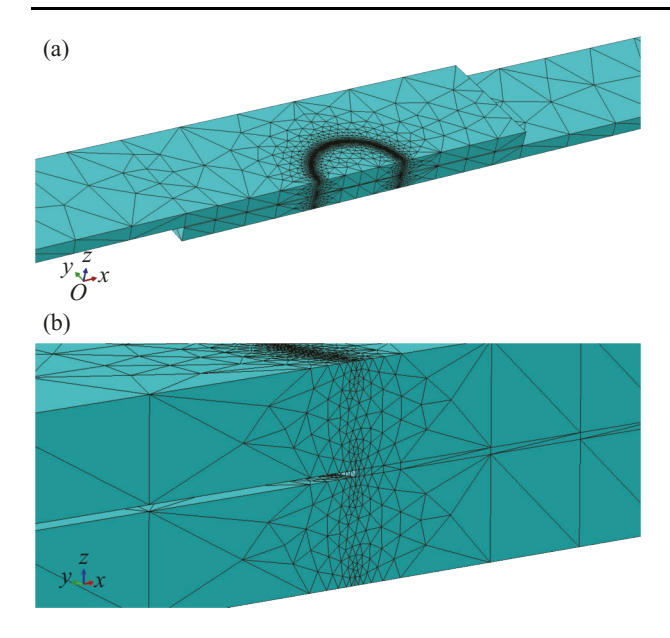


Fig. 2 FE mesh (a) The overall geometric setup and FE mesh used in this study (b) A close-up view at the end of the interlayer. This particularly example has a minimum mesh size of 100  $\mu$ m at the notch root

Table 2 Geometric parameter symbols and values varied in FE simulations

Interlayer radius <i>r</i> /mm	Interlayer thickness d/mm	Plate thickness t/mm	Plate width W/mm	Overlap area A/mm <sup>2</sup>
0.5, 1, 2, 3, 4, 5	0, 0.05, 0.1, 0.4, 0.6,0.8, 1, 1.6, 2	1.6	25	40

gaard<sup>[29]</sup>, the fracture energy  $G_c$  and the minimum mesh size e are related by  $G_c \approx (2-5)\sigma_0 e$  for N in the range of 0.2–0.4. Using material properties of  $\sigma_0 \cong 600$  MPa and  $G_c \cong 200$  kJ/m², the mesh size in the range of 66–166  $\mu$ m was estimated. Therefore, throughout this study, a minimum mesh size of 100  $\mu$ m was chosen in the location near the notch root as shown in Fig. 2 b.

# 2 Results from parametric study

A parametric study is conducted here to establish a relationship between failure mode and various geometrical parameters. Using the Buckingham Pi theorem, the non-dimensional parameters can be group into

Failure mode = 
$$\prod \left(\frac{r}{t}, \frac{d}{t}, \frac{a}{t}, \frac{w}{t}, f_{0,\text{plate}}, f_{0,\text{interlayer}}\right)$$
 (5)

where the geometrical parameters are normalized by the plate thickness t. Because  $a/t \gg 1$  and  $w/t \gg 1$ , these two parameters can be neglected.  $f_0$  is a parameter that indicates the initial porosity in the material. Base plate and inter-

layer porosity play a significant role in determining the failure mode. For the purposes of this work, the initial porosity  $f_0$  of both base plate and interlayer materials,  $f_{0,\text{plate}}$  and  $f_{0,\text{interlayer}}$  is taken to be 0.02, if not explicitly stated , which is usually used for ductile metals of moderate quality. The material properties are fixed to values tabulated in Table 1, and therefore no other parameters are involved in this equation. The final results are reported as a function of two main parameters, i.e., r/t and d/t.

The two failure modes can be illustrated by the representative results in Fig. 3. In these and other unshown simulations, failure initiates right after the peak on the force-displacement curve. In some extreme values of r/t and d/t, necking can be seen before noticeable fracture takes place. A more detailed discussion of such observations will be given later. Over a wide range of parameters, interfacial shear failure occurs for a small nugget size, e.g., r=2 mm in Fig. 3 a, while pull out failure is favoured for a large nugget size, e.g., r=5 mm in Fig. 3 b. As shown in Fig. 4, the dependence of failure force on the interlayer thickness d is quite weak until a large r/t is reached (e.g., as r/t > 2.5, re-

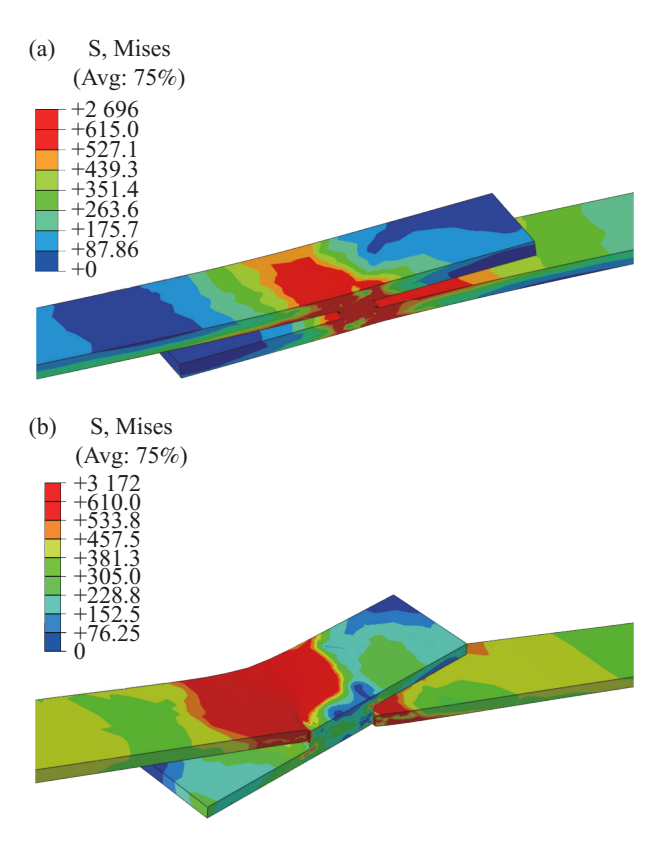


Fig. 3 The two failure modes (a) Interfacial shear failure for the case with r=2mm and d=1 mm, demonstrated by the Mises stress contours at 90% of the peak force after failure initiation (b) Pull out failure for the case with r=5 mm and d=0.1 mm, plotted at 80% of the peak force after failure initiation

duced interlayer thickness leads to an increase in failure force). Following the entire failure evolution, it has been found that due to the large plastic zone size, once started, the shear failure quickly propagates through the entire interlayer, while the pull-out failure localizes and forms two crescent-like cracks, followed by large rotation of the nugget and then tearing of the nugget completely from one plate.

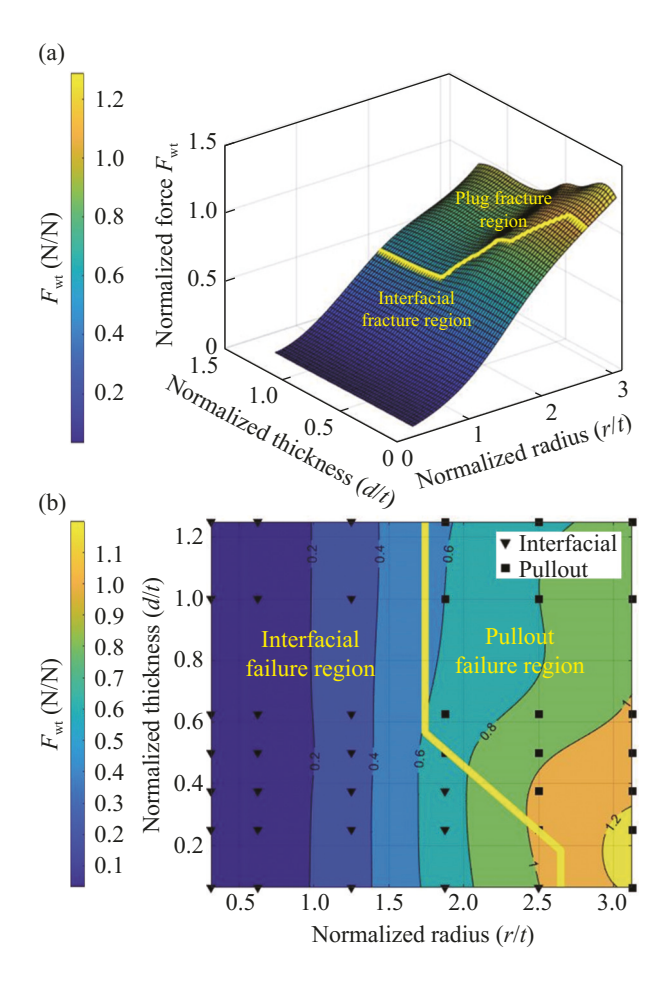


Fig. 4 The normalized force  $F_{wl} = \frac{F_{peak}}{\sigma_0 wt}$ , with respect to the two key geometric parameters, r/t and d/t, presented in the format of (a) a contour surface and (b) a 2D plot

The failure mode map can be described by a dimensionless analysis of the peak force. As nugget size and interlayer thickness constantly vary, it is convenient to normalize the force by yield strength, plate width and thickness, given by

$$F_{wt} = \frac{F_{peak}}{\sigma_0 wt} = \prod_{wt} \left(\frac{r}{t}, \frac{d}{t}, \cdots\right) \tag{6}$$

where only the two key dimensionless parameters are listed, i.e., r/t and d/t.  $F_{wt}$  is a dimensionless quantity defined as

normalized force in this paper. Further, as discussed in the introduction, the welding community models the critical force for interfacial shear failure by  $\sigma_s D^2$ , and that for pull out failure by  $\sigma_{UTS}Dt$ , where D is the diameter of spot joint,  $\sigma_s$  is the yield strength and  $\sigma_{UTS}$  is the ultimate tensile strength. Failure strength is an ill posed property, as it cannot be derived from either fracture mechanics or damage model for ductile metals. Nevertheless, for the sake of practicality, two additional dimensionless functions were proposed,

$$F_{Dt} = \frac{F_{\text{peak}}}{\sigma_{UTS}Dt} = \prod_{Dt} \left(\frac{r}{t}, \frac{d}{t} \cdots\right)$$
 (7)

$$F_{D^2} = \frac{F_{\text{peak}}}{\sigma_{UTS} D^2} = \prod_{D^2} \left( \frac{r}{t}, \frac{d}{t} \cdots \right)$$
 (8)

 $F_{\mathrm{Dt}}$  and  $F_{D^2}$  are dimensionless quantities that represent force normalized using  $\sigma_{UTS}Dt$  and  $\sigma_sD^2$ . Comparing these normalized peak force plots will allow evaluation of the validity of these simple strength equations from our mechanistic simulations of the entire failure processes.

The normalized peak force,  $F_{wt}$ , is given by the contour surface and 2D plots in Figs. 4 a and 4 b, respectively. The two failure modes are marked in Fig. 4 b by two different symbol types, and the boundary between these modes is delineated in all these plots. These results confirm that the primary factor controlling the failure mode transition is r/t, while the role of d/t is secondary. In our previous work of the two-dimensional counterpart [32], a similar dependence of normalized peak force on the normalized overlap size to Fig. 4 a has been seen. At small nugget size for 3D or small overlap size for 2D counterpart, the normalized peak force increases rapidly in the shear failure mode but approaches a plateau in the pull-out mode. An increase of the interlayer thickness promotes the pull-out failure despite a relatively weak dependence. This trend can be explained by the notch sensitivity. A large notch radius (corresponding to a large d/t) has reduced triaxial constraint on the deformation field of the interlayer, so that the tensile failure is easier to take place.

The surface plots for the normalized force  $F_{Dt}$  and  $F_{D^2}$  are shown in Figs. 5 a and 5 b, respectively. Under the assumption of failure strength (again, empirical and not mechanistic), the interfacial shear failure will take place when  $F_{D^2}$  reaches a critical high value, and so does the pull-out failure (i.e., plug fracture) as  $F_{Dt}$  reaches a critical value. The overall observations of large  $F_{D^2}$  at low r/t and large  $F_{Dt}$  at high r/t appear to agree with this line of argument, which is the essential reason for the prior success of such models in AWS compiled data. However, one would not be able to extract critical values for these two normalized

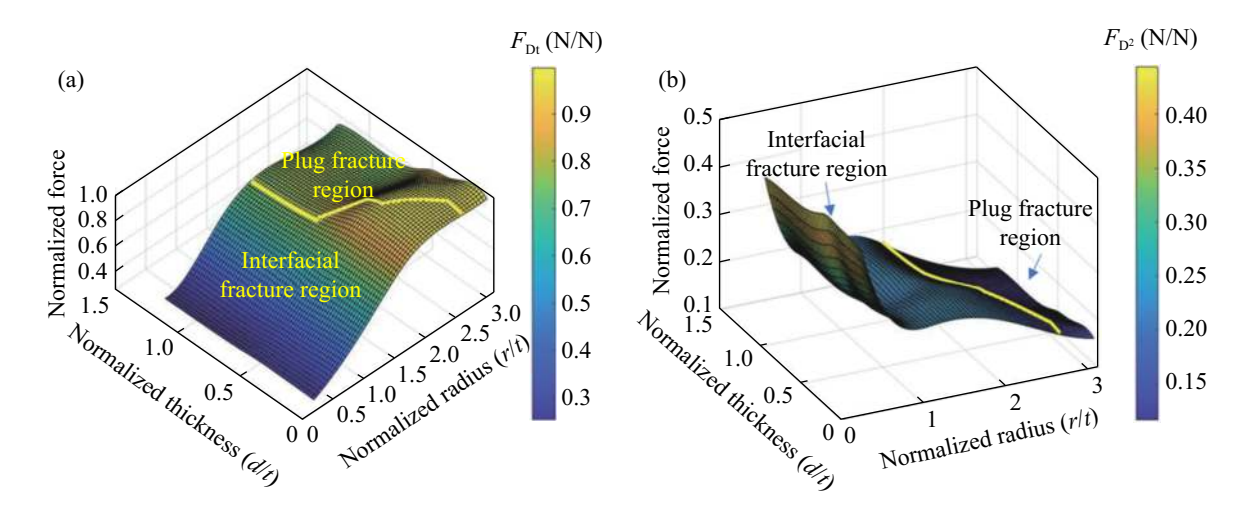


Fig. 5 Surface plots of (a) the normalized force,  $F_{Dt}$ , and (b) normalized force,  $F_{D^2}$ 

forces, as these two forces never reach any plateaus, which again arises from the improper usage of a critical strength criterion for the failure of ductile metals.

From the above analysis, it is found that a complete parametric study based on GTN damage analyses is rather cumbersome because of the fine mesh requirement and various possible void-nucleation mechanisms. To circumvent this challenge, we notice that a no-damage model should set up an upper bound of the load-bearing capacity of the boundary value problem in Fig. 1. In this case, as the material continues to harden as in Eq. (1), the reason for the occurrence of a peak force is of geometric origin, i.e., the two failure modes are simply preceded by necking. In the nodamage model with small nuggets, shear failure is manifested by severe stretching, thinning, and necking of the joint zone. For large nuggets with pull-out failure, the corresponding no-damage simulations show the nugget rotation and necking of the plate material near the nugget zone. Results for no-damage simulations are overlaid with the damage-based analyses in Fig. 6. The calculated peak force  $F_{\rm wt}$ 

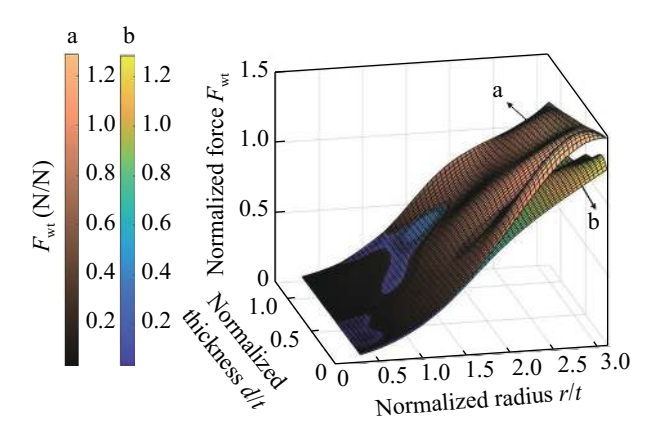


Fig. 6 Surface plots of  $F_{\it wt}$  for no-damage model (a) and GTN model (b)

is not much different between GTN and no-damage analyses, and better agreement is shown in the small nugget region. Note that in this set of parametric studies, plate and interlayer porosity  $(f_0)$  is set to be 0.02.

# 3 Comparison with the prior spot-weld experiments

The parametric study shows a strong dependence of peak force on the nugget radius and a weak dependence on the interlayer thickness. The former has been routinely seen in the welding community. Here a comparison will be made to our previous tensile shear tests on spot-welded lap joints of galvannealed DP980 steels using a specially designed HEA filler interlayer with varying thickness for the purpose of liquid metal embrittlement control<sup>[18]</sup>.

During the spot-welding process, the localized high heat input changes the material microstructure and thus the mechanical properties. To capture this variation, a Vickers hardness line scan was performed on the welded sample, showing an elevated hardness in the nugget zone and a significant softening in the heat affected zone (HAZ). Following[30, 33 - 34], we adopt a proportional relationship between the measured hardness and yield strength in our model setup. As a material strength gradient is not allowed in ABAQUS, the model geometry is divided into six zones with each zone assigned a homogeneous material property, as shown in Fig. 7. The mesh size in each zone varies according to the zone width and follows the GTN mesh requirement. The yield strength and tensile strength in the nugget region is estimated base on the localized hardness ratio. The hardness/strength ratios from zone 1 to 6 are 1.51, 1.19, 0.94, 0.95, 0.98 and 1.00, respectively. Such settings lead to about 50% increase of the total number of elements when compared to the setup in Fig. 2.

Comparing the deformation snapshot in Fig. 8 to the

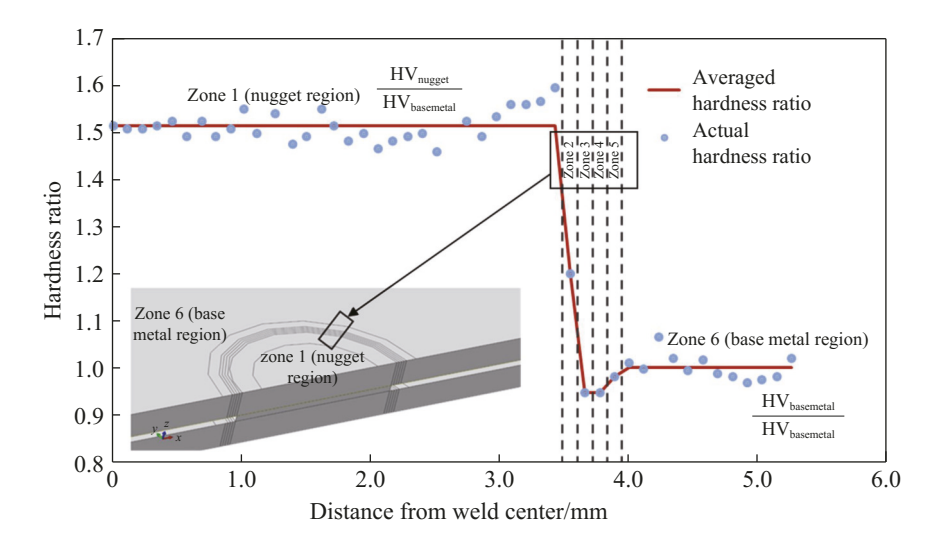


Fig. 7 The material hardness and strength vary significantly from the nugget to the base metal, with HAZ being the softest region. Six zones were set up in the FE model, each of which has a homogeneous material property. The mesh size varies according to the zone width and follows the GTN mesh requirement

contours associated with a single failure mode in Fig. 3 a and b, the failure mode for the DP980 spot weld with r=4 mm and d=220 µm initiates with partial pull-out and partial interfacial shear, and later evolves into full pull-out fracture. This prediction agrees well with our previous experimental observation<sup>[18]</sup>. This interlayer effect can be understood from the complex stress state due to geometric constraints<sup>[7,35]</sup>. The stress state near the periphery of the filler interlayer, like in a notch, will be a sum of shear and hydrostatic tension at the beginning. Upon rotation of the nugget zone, the stress state evolves into a sum of a uniaxial tension and a large hydrostatic component. The classic Bridgman analysis showed the reduction of the hydrostatic component when the notch size (here the interlayer thickness)

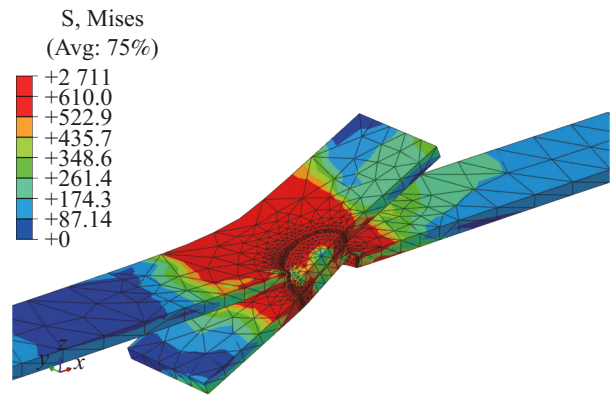


Fig. 8 The failure mode is initially a mixture of interface shear and pull-out slightly after the peak force, but soon evolves into the pull-out fracture as shown here at 30% of the peak force near the final stage. The mesh setup follows Fig. 7 with r = 4 mm and d = 220  $\mu$ m.

increases. As long as the interlayer thickness is much smaller than the nugget size, this stress state change is not deemed to be large. Nevertheless, both experiments and simulation results show consistently and quantitatively such a subtle dependence.

Fig. 9 summarizes and compares the peak force calculated from the models and tensile shear tests with respect to a range of d = 220, 240, 270, and 370  $\mu$ m. Using a porosity of  $f_0 = 0.02$ , the calculated normalized peak force  $F_{wt}$  is generally lower than the experimentally measured values, while the no-damage model over predicts. A choice of  $f_0 = 0.01$  leads to a good agreement with the previous experi-

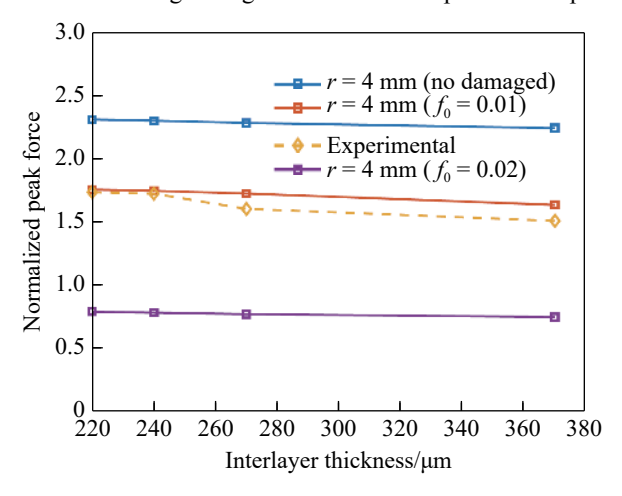


Fig. 9 The normalized peak force  $F_{wt}$  with respect to the interlayer thickness for  $f_0 = 0$ , 0.01 and 0.02, respectively.  $f_0 = 0.01$  yields a good agreement with previous experimental results<sup>[18]</sup>, indicating the mere consideration of stress analysis can nicely predict the failure mode and force

mental results<sup>[18]</sup>, but no further attempt is made to improve the agreement as  $f_0$  by itself is quite sensitive to material processing. All the three calculated curves predicted a slight reduction of peak force with increasing filler interlayer thickness. It can be concluded that when intermetallic phase is out of the question, the mere stress analysis is found to be successful in predicting both the failure mode evolution and quantitatively the failure force.

### 4 Conclusions

- (1) Two failure modes, namely interfacial shear failure and pull-out fracture, are generally observed during tensile shear tests on spot-welded lap joints.
- (2) A complete parametric study was performed to reveal the failure initiation and evolution during lap shear tests, based on the GTN damage model.
- (3) Both the peak force and fracture mode showed a strong dependence on the ratio of the size of the spot weld (i.e., radius) to the plate thickness, while the dependence on the interlayer thickness was minor but consequential over a large range.
- (4) The no-damage model exhibits similar trends and can be used for a fast evaluation of peak force dependence without the loss of predictability.
- (5) The predicted dependence of joint strength on the interlayer thickness is validated by a good agreement to our previous spot-welding experimental results, in which the joint region was free of intermetallic phases and therefore avoided complications in the failure analysis.

# References

- [1] Shirzadi A A. Diffusion bonding aluminium alloys and composites: new approaches and modelling. Doctoral thesis, Kings college, University of Cambridge, United Kingdom, 1997.
- [2] Gale W F. Applying TLP bonding to the joining of structural intermetallic compounds. JOM, 1999, 51(2):49 52.
- [3] Lienert T, Siewert T, Babu S, Acoff V. Summary of fusion welding processes. Welding Fundamentals and Processes 6A, ASM International, 2011.
- [4] Hutchinson J W, Suo Z. Mixed mode cracking in layered materials. Advances in applied mechanics. 1992, 29(1): 63-85
- [5] Flom Y. Strength and margins of brazed joints. Advances in Brazing: Science, Technology and Applications, 2013.
- [6] Flom Y. Evaluation of brazed joints using failure assessment diagram. IBSC 2012 - Proceedings of the 5th International

- Brazing and Soldering Conference, 2012, 129 132.
- [7] Riggs B, Benatar A, Alexandrov B T, Xu R. Experimental validation of damage zone models for lap shear brazed joints using DIC. Welding Journal, 2017, 96(8): 421–428.
- [8] Han J H, Ahn J P, Shin M C. Effect of interlayer thickness on shear deformation behavior of AA5083 aluminum alloy/SS41 steel plates manufactured by explosive welding. Journal of Materials Science, 2003, 38(1):13 – 18.
- [9] Chawla N, Shen Y L, Deng X, et al. An evaluation of the lap-shear test for sn-rich solder/Cu couples: Experiments and simulation. Journal of Electronic Materials, 2004, 33(12):1589 – 1595.
- [10] Erskine K M, Meier A M, Joshi V V, et al. The effect of braze interlayer thickness on the mechanical strength of alumina brazed with Ag-CuO braze alloys. Advanced Engineering Materials, 2014, 16(12):1442 1447.
- [11] Nielsen K L. 3D modelling of plug failure in resistance spot welded shear-lab specimens (DP600-steel). International Journal of Fracture, 2008, 153(2):125 139.
- [12] Mortazavi S N, Marashi P, Pouranvari M, et al. Investigation on joint strength of dissimilar resistance spot welds of Aluminum alloy and low carbon steel. Advanced Materials Research, 2011, 264:384 389.
- [13] Pouranvari M, Asgari H R, Mosavizadch S M, et al. Effect of weld nugget size on overload failure mode of resistance spot welds. Science and Technology of Welding and Joining, 2007, 12(3):217 225.
- [14] Chen R, Lou M, Li Y, Carlson B E. Improving weldability of Al-Si coated press hardened steel using stepped current pulse schedule. Journal of Manufacturing Processes, 2019, 48:31 – 43.
- [15] Chen R M, Zhang C Q, Lou M, et al. Effect of Al-Si coating on weldability of press-hardened steels. Journal of Materials Engineering and Performance, 2020, 29(1):626 636.
- [16] Tavasolizadeh A, Marashi S P H, Pouranvari M. Mechanical performance of three thickness resistance spot welded low carbon steel. Materials Science and Technology, 2011, 27(1):219 224.
- [17] Pouranvari M, Marashi S P H, Safanama D S. Failure mode transition in AHSS resistance spot welds. Part II: Experimental investigation and model validation. Materials Science and Engineering A, 2011, 528(29–30): 8344–8352.
- [18] Abdelmotagaly A. High entropy alloy interlayers for mitigation of liquid metal embrittlement in galvannealed advanced high strength steel welds. MS Thesis, Colorado School of Mines, 2020.
- [19] Radakovic D J, Tumuluru M. Predicting resistance spot weld failure modes in shear tension tests of advanced high-strength automotive steels. Welding Journal, 2008, 87(4): 96 105
- [20] Da Silva L F M, Das Neves P J C, Adams R D, et al.

- Analytical models of adhesively bonded joints-Part I: Literature survey. International Journal of Adhesion and Adhesives, 2009, 29(3):319 330.
- [21] Da Silva L F M, Das Neves P J C, Adams R D, et al. Analytical models of adhesively bonded joints-Part II: Comparative study. International Journal of Adhesion and Adhesives, 2009, 29(3):331 341.
- [22] Radaj D, Zhang S. Simplified formulae for stress intensity factors of spot welds. Engineering Fracture Mechanics, 1991, 40(1):233 236.
- [23] Yang J, Su J H, Yu Z S, et al. Influence of Ni interlayer width on interfacial reactions and mechanical properties in laser welding/brazing of Al/Mg lap joint. Science and Technology of Welding and Joining, 2020, 25(1):37 44.
- [24] Zhou F, Jiang W C, Tom J N, et al. Crack propagation of SS304/BNi-2 brazed joints: Experiments and numerical simulations. Metals, 2019, 9(10):1031.
- [25] Zhang S. Stress intensities at spot welds. International Journal of Fracture, 1997, 88(2):167 185.
- [26] Sarrado C, Albert T, Costa J, et al. On the validity of linear elastic fracture mechanics methods to measure the fracture toughness of adhesive joints. International Journal of Solids and Structures, 2016, 81:110 116.
- [27] Shahani A R, Abolfathitabar R, Shooshtar H. On the validity of LEFM methods to investigate the fracture behavior of angle-ply laminates. Composites Part B:Engineering, 2019,

- 160:249 253.
- [28] Campilho R D S G, Banea M D, Pinto A M G, et al. Strength prediction of single- and double-lap joints by standard and extended finite element modelling. International Journal of Adhesion and Adhesives, 2011, 31(5):363 372.
- [29] Tvergaard V. Material failure by void growth to coalescence. Advances in Applied Mechanics, 1989, 27:83 151.
- [30] Nielsen K L. Ductile damage development in friction stir welded aluminum (AA2024) joints. Engineering Fracture Mechanics, 2008, 75(10):2795 2811.
- [31] Shojaei Zoeram A, Akbari Mousavi S A A. Effect of interlayer thickness on microstructure and mechanical properties of as welded Ti6Al4V/Cu/NiTi joints. Materials Letters, 2014, 133:5 – 8.
- [32] Gao Y, Xue Z, Yu Z. Failure mode maps of lap joints under the tensile shear testing condition. Extreme Mechanics Letters, 2020, 37:100728.
- [33] Nielsen K L, Tvergaard V. Ductile shear failure or plug failure of spot welds modelled by modified Gurson model. Engineering Fracture Mechanics, 2010, 77(7):1031 1047.
- [34] Rezayat H. The role of heterogeneous constitutive properties on mechanical behavior of advanced high strength steel spot welds. Knoxville: University of Tennessee. 2019.
- [35] Flom Y, Wang L. Flaw tolerance in lap shear brazed joints part 1. Welding Journal, 2004, 83(1):32 38.